Ion mobility–mass spectrometry of supramolecular complexes and assemblies

Elina Kalenius[a]*, Michael Groessl[b] and Kari Rissanen[a]*

[a]Department of Chemistry, University of Jyväskylä, Jyväskylä, Finland.
[b]Department of Nephrology and Hypertension, Department of BioMedical Research, Inselspital, Bern University Hospital, University of Bern, Bern, Switzerland

*Email: elina.o.kalenius@jyu.fi; kari.t.rissanen@jyu.fi

Abstract | Despite their structural and functional differences, synthetic supramolecular assemblies share many similarities with biological ones, especially enzymes. The assemblies can be on the same length scales, and their structures and guest binding are typically governed by non-covalent interactions. Thus, only relatively weak interactions define the shape of a synthetic supramolecule or a protein's secondary and tertiary structure, such that the resulting dynamism makes structure elucidation challenging. In the case of biomolecules such as peptides, proteins, glycans and lipids, this has often been tackled using ion mobility-mass spectrometry (IM-MS), whereby analyte ions are separated according to their gas-phase mobility as well as their mass-to-charge ratio. IM-MS is an established method in 'omics', separation sciences, and small molecule structural chemistry but has only recently grown in popularity for the study of synthetic supramolecular assemblies in the gas phase. This Perspective describes IM-MS techniques and how they help us understand the structures of molecular self-assemblies, host–guest complexes and metallosupramolecular complexes.

[H1] Introduction

The accurate determination of molecular structure is a nontrivial challenge in supramolecular chemistry. If the weakly bound assemblies order themselves in the solid state, then single crystal X-ray diffraction affords arguably the most spatially accurate structural model for this state[2]. When on a solid surface, the assemblies can be amenable to ultra-high resolution microscopy techniques, which allow us to study inter- and intramolecular interactions on solid surfaces.[9] These experiments provide detailed information about self-assembly thermodynamics of multi-component systems, as well as highly complex fractal-like and quasicrystalline 2D systems. When in solution, assemblies can adopt different structure(s), which can often be teased out using NMR spectroscopy, in particular diffusion NMR techniques such as diffusion ordered spectroscopy (DOSY)[1]. DOSY NMR gives reliable information on the effective size of molecular species, including supramolecular assemblies and host–guest complexes. For example, the sizes of molecular capsules and cages — species that can be labile and exist as multiple oligomers/conformers — can be confirmed in solution using this method.[3–5] This structural information is well complemented by quantitative data regarding the strengths of the

supramolecular interactions, data that typically involve titrating the molecular components and determining their speciation using NMR, UV-visible and/or fluorescence spectroscopies.[6] These methods, as well as other solution techniques such as isothermal titration calorimetry (ITC), can be used to study cooperative aggregation, intermolecular (allosteric) cooperativity, intramolecular (chelate) cooperativity and interannular cooperativity in supramolecular systems.[7] Accurate information regarding the dimensions of any ions in the gas phase had been elusive until the development of ion mobility-mass spectrometry (IM-MS; also referred to as ion mobility spectrometry-mass spectrometry, IMS-MS). An IM analyser separates ions according to their mobility through carrier gas, and this parameter can be linked to the dimensions of an ion. The separated ion(s) then pass through a conventional mass analyser, and the instrumentation to carry out this tandem analysis is described in the next section. IM-MS is thus a hyphenated method that can, for example, distinguish ions that are isomeric (have the same mass-to-charge ratio m/z) but have different sizes. Although IM-MS measurements are mainstream in the characterization of certain biomolecules, the adoption of IM-MS by the supramolecular chemistry community has only come more recently, which is surprising given such chemistry often features large molecules in different conformations or aggregation states (for example, equilibrium between oligomers $[M_m]^{mx+} \leftrightarrow [M_n]^{nx+}$ is common). This Perspective highlights abiotic supramolecular assemblies for which IM-MS has played a crucial role in structure elucidation. We will first introduce the technique in the context of biomolecular characterization, more detailed treatments of which can be found in recent reviews.[10–14] Instead, we move to how IM-MS can address structural ambiguity in supramolecular assemblies, particularly in metallosupramolecular and host–guest chemistry.

[H1] Instrumentation

Before being subjected to IM-MS, an analyte must first be ionized and brought into the gas phase (FIG. 1a). In the context of supramolecular chemistry, this is often achieved using electrospray ionization (ESI), a versatile and soft ionization method. This and other common ion sources such as atmospheric pressure chemical ionization (APCI), atmospheric pressure photoionization (APPI) and matrix assisted laser desorption ionization (MALDI) have been compared elsewhere.[32] The choice of ionization is made according to how strong a signal-to-noise ratio one can achieve while still maintaining the structural integrity of an analyte. In the case of characterizing labile structures such as supramolecules, ESI is often the method of choice because it can result in charging and ion transfer to gas phase without disrupting the non-covalent inter- or intramolecular interactions holding the assemblies together. The intact ions are then subjected to IM analysis, the principles of which can be traced back to the 19th century, even though application to chemistry only became widespread in the 1960s.[9,15] Mass spectrometers can typically be combined (‘hyphenated’) with one of three different types of IM spectrometer: drift-tube IM (DTIM), travelling wave IM (TWIM) and trapped IM (TIM). These spectrometers are technically distinct but can each enable a structural analysis. Each type is currently

commercially available from the following manufacturers (model): Agilent (6560)[16], Bruker (timsTOF^{TM}),[17] Tofwerk (IMS-TOF)[18] and Waters (Synapt G2-Si)[19]. A detailed technical comparison between these and other ion mobility techniques is beyond the scope of this Perspective, but readers seeking more information on ion mobility principles and instrumentation are well served by recent articles.[9,11,12,21] We now offer a concise introduction to the IM methods of relevance to structural supramolecular chemistry.

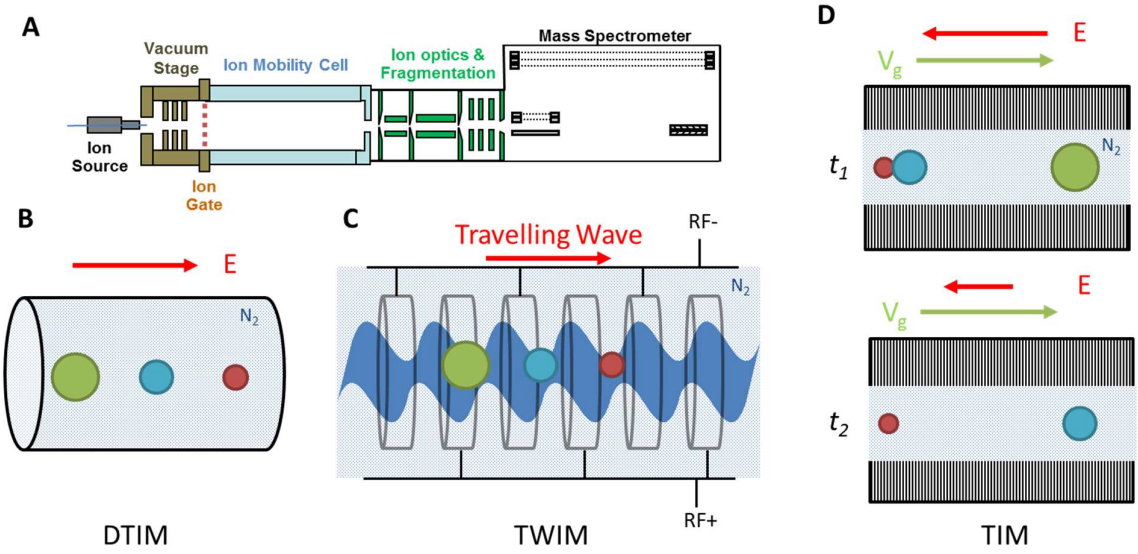

Figure 1 | **Layout of an ion mobility-mass spectrometer and common ion mobility cells. A** | A typical configuration of instrument for ion mobility-mass spectrometry (IM-MS) has the analytes first passing through an ionization source before encountering a low-pressure stage (usually around 3 mbar). The charged and desolvated analytes then pass through an ion gate into the IM cell, where they undergo collisions with a buffer gas such as N_2. The ions, now sorted according to their collision cross-section, can now be subjected to mass spectrometry (MS), with the option of prior fragmentation (MS/MS). Another setup is also possible, in which the ion optics and fragmentation precede the IM cell. **Ba** | The simplest IM system is a DTIM analyzer, through which analyte ions drift while encountering a static uniform electric field. Here, the red analyte experiences the least number of collisions and elutes first. **Bb** | In TWIM instruments, the ions are focused through a set of rings with alternate polarizations. Additionally, a travelling potential wave is applied, which separates the analyte ions according to their size and shape. Once more, the small, red analyte elutes first. **Bc** | In TIM, ions are trapped by an electrostatic force in one direction and a flow of buffer gas in the opposite direction. By slowly reducing the strength of the electric field, ions can sequentially elute from the cell. Note, here it is the larger green analyte that elutes first, because the buffer gas 'pushes' it the most. E = electric field; t_1 and t_2 = consecutive time points.

The oldest and simplest IM analyzer is a drift-tube IM (DTIM), over which a static uniform electric field is applied to drive ions from one end of a gas-filled tube to the other. Over the period spent traveling through the IM drift tube — known as the drift time t_d — each ion undergoes collisions with the buffer gas. The different ion geometries and ion–gas interactions contribute to an averaged observable value known as the collision cross section (CCS).[10] The CCS is indicative of an ion's size and shape, being smaller for compact or spherical molecular structures and larger for extended or unfolded structures. For example, two different conformations of an ion can have quite distinct CCS values. The CCS value measured for a certain ion in a certain conformation will be the same for a given buffer gas temperature/pressure and electric field. It can therefore be used as a structural identifier, which can be compared to data obtained using other techniques such as single crystal X-ray diffraction and DOSY NMR. A more precise relationship between CCS and structure can be had by comparing experimental CCS values with calculated ones.[22–25] Once t_d has been measured for a given species, it can be combined with other known experimental parameters to compute the CCS according to the Mason–Schamp equation (eq. 1):[9]

$$\Omega = \frac{3}{16}\left(\frac{2\pi}{\mu k T}\right)^{1/2}\frac{qzEt_d}{LN} \qquad \text{Equation 1}$$

where Ω is the integrated CCS, μ is the reduced mass of the ion and the drift gas, k_B is Boltzmann's constant, q is the elementary charge, z is the charge of the analyte ion, E is the magnitude of the electric field, L is the length of the drift tube and N is the number density of the buffer gas. When the DTIM system operates at low electric field one can directly obtain the most precise CCS values.[26] Moreover, DTIM can achieve relatively high resolving power ($R = \Omega/\Delta\Omega > 100$), such that one can routinely separate two ions whose CCS values differ by only 1%.

The DTIM analyzer is conceptually simple because it involves only a static electric field. Travelling wave IM (TWIM) also requires a (low-pressure) drift tube but makes use of a travelling voltage applied to a series of ring electrodes.[27] The ions pass only through the centre of the ring electrodes because they are held at opposite-phase radio-frequency voltages. Additionally, a direct voltage is applied to one ring electrode after another to set up the travelling potential wave. Small, high-mobility ions 'surf' the wave and quickly traverse the tube whereas large, low-mobility ions require more waves to get to the end. The constantly changing voltage experienced by the ions means that equation 1 does not hold for TWIM. Consequently, the technique affords relative rather than absolute data. Indeed, a TWIM analyzer has to be calibrated with standard ions that are structurally robust in the gas phase and have physical properties — mass, charge and ion–dipole interactions with the drift gas — that are very similar to those of the analyte ion. Many standard peptides, glycans and lipids are available, to which one can compare unknown species of the same type. However, such standards are not available for most supramolecular systems, such that the technique is potentially less broadly applicable.[28] Moreover, the

low resolving power of TWIM ($\Omega/\Delta\Omega = 40$) is often insufficient to discriminate between closely related ion structures such as stereoisomers and conformers.

The newest IM technique that we will describe here is trapped ion mobility (TIM) spectrometry,[17,29] a method that first involves trapping ions using radially-confining radio-frequency electric fields. The ions are then separated by slowly changing the balance between an axial electric field and an opposing flow of carrier gas. As the electric field is decreased, the drag force on the analyte ions predominates and the ions elute from the TIM analyzer. One can easily change the electric field in a gradual manner, such that high resolving power can be achieved ($\Omega/\Delta\Omega > 200$).[30] As with TWIM, CCS determination using TIM requires calibration with standards of known CCS.

IM data are typically communicated as plots of intensity versus t_d, with the peak widths being typically on the order of ~ms. These narrow widths mean that the MS measurements that follow must be sufficiently fast to keep up with IM separations, especially if analyte ions have similar t_d values. As with the choice of ionization source, the choice of mass analyzer is in principle open.[11] However, TIM-, DTIM- and TWIM-MS instruments almost exclusively feature time-of-flight (TOF) mass analyzers because these allow one to record spectra on a ~μs timescale. Some of these instruments also include a quadrupole mass analyzer prior to the TOF analyzer (as in FIG. 1) or prior to the IM cell. In this qTOF-MS configuration, the quadrupole allows ions within a narrow mass-to-charge ratio (*m/z*) range to be pre-selected and isolated prior to being subjected to fragmentation — referred to as MS/MS, MS^2 or collision induced dissociation (CID). The resulting spectra feature *m/z* values that correspond to fragment ions, whose structures better allow us to identify the structure of the parent ion. Instruments also exist that can perform so-called post IM all-ion fragmentation, whereby all ions are simultaneously fragmented. Because this occurs after IM separation, the fragment ions can be assigned to their precursors based on identical IM drift times.[31] In the case of a TIM analyzer, the elution of ions can be sufficiently slow such that they can be efficiently processed by a Fourier-transform ion cyclotron resonance (FT-ICR) mass spectrometer. This analyzer requires long scan times but enables very high mass resolution.[30]

[H1] Background: biological supramolecules

It was only shortly after the commercialization of IM-MS instruments that the technique became widely adopted by the biophysical and structural biology communities. One reason for this may be higher sensitivity of MS relative to other biophysical techniques. Analyte ions can usually be detected at mid-nM concentrations and only a few μL of sample are needed. In contrast to NMR spectroscopy or single crystal X-ray diffraction, sample purity is much less of a concern because the ions of interest can be isolated even from complex biological matrices. Additionally, although single crystal X-ray diffraction is unrivalled in terms of spatial resolution of biomolecular structure, it only provides static information. In contrast, if one measures CCS values of a biomolecule under different conditions, IM-MS can

provide a dynamic picture of a protein binding a ligand or undergoing folding and unfolding (or other conformational changes).[12,33] For example, there now exists an elegant IM-MS assay to quantify the stabilizing effect that ligand binding has on the folded state of a protein.[34] The protein–ligand complex can be subjected to collisional activation in order to induce unfolding, as signaled by an increased CCS value. If the stabilizing effect is large, one requires a high collision energy to unfold the protein, as can be quantified using dedicated data analysis software[34]. In contrast to most solution-based assays, this approach allows the interrogation of membrane protein–lipid complexes, which are notoriously difficult to characterize by single crystal X-ray diffraction.

As we have noted, non-covalent protein–ligand interactions can be studied by probing subtle conformational changes using IM-MS.[35] For example, it is possible to monitor, in real time, the binding of small molecules to peptide deformylase, an enzyme that catalyzes the reversible hydrolysis of N-terminal N-formylated Met to give the N-terminal Met and formate. Expressed in pathogenic prokaryotes, the enzyme is considered a promising target for small molecule antibiotics — inhibitors that bind the enzyme and induce it to fold from an open (O) to a closed conformation (C) (FIG. 2). Because binding and reorganization are relatively slow, one can continuously measure the CCS of the protein–ligand complex during the process, such that one can extract rate constants. However, in this and other cases, extreme care has to be taken to ensure that the conformation(s) and composition of a protein in solution are undisturbed when it is brought into the gas phase. The CCS value determined by IM-MS for a protein in a low charge state is always smaller than that calculated from the corresponding crystal structure. Conversely, IM-MS of a protein in a high charge state affords a higher CCS because of Coulombic repulsion between residues.[36] Moreover, algorithms for calculating CCS from crystal structures are susceptible to errors because they cannot accurately model the complex interactions between ions and the buffer gas.[37]

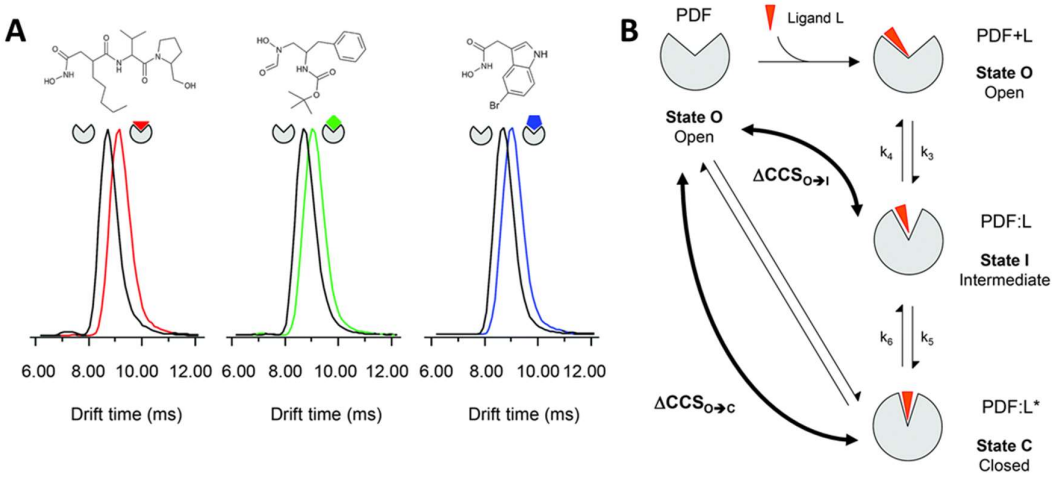

Figure 2 | **Non-covalent interactions between peptide deformylase (PDF) and three bacterial PDF inhibitors monitored by TWIM-MS. a** | When PDF binds a small molecule the protein undergoes structural changes, as evidenced by a change in IM drift time. The increases in drift time correspond to an increase in collision cross section of about 1%. **b** | A schematic describing how a slow (on the timescale of minutes) tight binding process can be monitored by IM-MS. $\Delta CCS_{O\rightarrow I}$ and $\Delta CCS_{O\rightarrow C}$ are the differences between the collision cross sections of the open (O) and semi-closed (I), and open and closed (C) conformations, respectively. Figure reproduced with permission from REF. 35, Royal Society of Chemistry.

[H1] Host–guest complexes

It is not only proteins that can play host to small molecules. Indeed, large synthetic architectures can also bind molecules, and host–guest chemistry is of interest for applications in sensing, transport and catalysis.[38–41] In order for the host to function, it must present a binding site with structural integrity. We will introduce IM-MS in host–guest chemistry first in the context of simple organic hosts such as cucurbiturils and cyclodextrins — two cyclic species that feature hydrophobic interiors and bind organics. For example, one early IM-MS study made use of a custom-built spectrometer to probe the binding of lysine (Lys) to macrocyclic hosts cucurbit[5]uril (CB[5]), cucurbit[6]uril (CB[6]) and α-cyclodextrin (α-CD)[12]. It is important to perform IM-MS, as well as the accompanying sustained off-resonance collision-induced dissociation (SORI-CID) experiments and theoretical calculations, because the guest can bind in an *endo* or *exo* mode. Complexes $[CB[5]+Lys+H]^+$ and $[CB[6]+Lys+2H]^{2+}$ showed single peaks in their IM arrival time distributions. Comparison of experimental and theoretical CCS values showed *exo* complexation for singly charged Lys with CB[5] (CCS_{exp} 184 Å^2, $CCS_{theor,exo}$ 170 Å^2 and $CCS_{theor,endo}$ 186-187 Å^2), whereas threaded *endo*-structure was formed with CB[6] and doubly charged Lys (CCS_{exp} 189 Å^2, $CCS_{theor,exo}$ 193 Å^2 and $CCS_{theor,endo}$ 218-225 Å^2). Arrival time distribution for complex of α-CD with Lys showed two peaks with distinctively different drift times (620 and 770 μs), which originate from dimer $[\alpha\text{-CD}+Lys+H]_2^{2+}$ and monomer $[\alpha\text{-CD}+Lys+H]^+$ where Lys is attached on rim of cyclodextrin (having either salt-bridged or charge solvated structure). Dimer and monomer have same *m/z* values and would be difficult to separate without IM-analysis. This study was followed by more work on inclusion complexes, including TWIM-MS on inclusion complex formation of cucurbiturils has become more active. IM-MS applications to study alkyl diammonium guests,[42,43] amino acids,[44] and peptides[45] in cucurbiturils and anions within hemicucurbiturils. Ensuring *endo* binding inside host molecule is of particular importance if supramolecular hosts are to be used as nanocontainers or nanocatalytic devices. In the case of CB[6–8],[46] TWIM-MS could be used to confirm *endo*-complexation of the azoalkane guest 2,3-diazabicyclo[2.2.2]oct-2-ene (**1**) as well as to follow the fragmentation of **1** inside the CB[*n*] (FIG. 3a). The latter was made possible by using an IM-MS instrument (for example, the Waters Synapt) equipped with quadrupoles for ion isolation and activation prior to IM and MS analyses. The drift times of the protonated host $[CB[7]+H]^+$ and its complex

[CB[7]+**1**+H]$^+$ are virtually identical, such that *endo*-complexation is clear without even determining the CCS values. The drift times of [CB[7]+H]$^+$ and *endo*-[CB[7]+**1**+H]$^+$ are expected to be similar and considerably lower than that of *exo*-[CB[7]+**1**+H]$^+$, an ion that is estimated to have a ~10 Å^2 larger CCS.

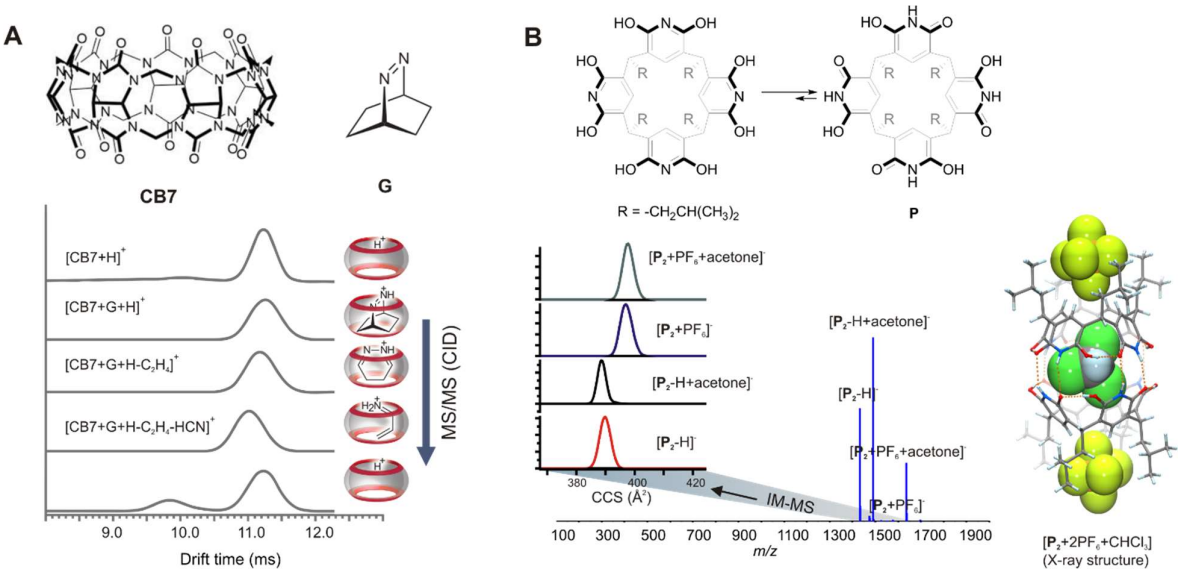

Figure 3 | ***Endo*/*exo*-complexes of organic hosts and guests are distinguishable by ion-mobility mass spectrometry. Aa** | The complexation of cucurbit[7]uril with hydrophobic azo compound **1** studied using travelling wave ion mobility spectrometry. **Ab** | The main IM signal for [CB[7]+H]$^+$, [CB[7]+**1**+H]$^+$ and the fragment ions after collision-induced dissociation of [CB[7]+**1**+H]$^+$. The drift times of each ion are similar, with those of the smaller guests being slightly smaller due to contraction of the host. **Ba** | Bowl-shaped pyridine[4]arene **2** exists primarily as its amide tautomeric form. dimerizes *exo*-complexation of dimer: **Ba** | ESI-MS spectrum for equimolar **2** and ^{n}Bu$_4$NPF$_6$ in acetone, with DT-IM arrival time distributions shown for selected ions. The anion complex of dimer is also observed in the crystal structure of [**2**$_2$+CHCl$_3$+2PF$_6$]$^{2-}$. Part **a** reproduced with permission from REF. 46, Springer Nature. Part **b** reproduced with permission from REF. 47, Wiley-VCH.

Being confident of the structure of [CB[7]+**1**+H]$^+$, this ion was then subjected to collision induced dissociation (CID) experiment, in which pre-determined ion is isolated, accelerated by a potential offset (in quadrupole mass analyzers) and allowed to collide with inert gas (typically N_2, He or Ar) leading to ion activation, increase of internal energy and finally ion fragmentation/dissociation. During the CID experiment of [CB[7]+**1**+H]$^+$ the guest stays in the container but undergoes *retro*-Diels–Alder reactions, extruding C_2H_4 to give [CB[7]+pyridazine+H]$^+$ and then HCN to give [CB[7]+1-azabutadiene+H]$^+$. The fragmentation of the guest causes the host to contract slightly in order to strengthen its interactions with its now smaller guest. Complete dissociation gives back [CB[7]+H]$^+$, indicated by the drift time and

MS data being the same for the free host. We stress again that a disadvantage of TWIM-MS is that it does not allow accurate CCS determination without data for comparable molecules with known CCS values.[28] Nevertheless, even without this lack of absolute data in the absence of a calibrant, relative drift times still give structural information in this case because empty host ions $[CB[n]+H]^+$ can serve as reference ions. In a related example of IM-MS and CID analysis of CB[*n*] systems, these methods were combined with calculations to investigate *endo*/*exo*-complex formation between a CB[6] host and 1,4-diaminobenzene guest.[66] As expected, the kinetic product is an *exo* species that can rearrange to the thermodynamically preferred *endo*-complex. It was found that solution self-assembly, while accelerated with temperature, requires a surprisingly long time to reach equilibrium, enabling one to monitor the complexation using IM-MS and CID.

Let us now move to a situation in which IM-MS analysis is even more valuable, a situation where *endo* and *exo* complexation modes feature in the same self-assembled structure, as is the case for a capsule comprising two pyridine[4]arene bowles (**2**, FIG. 3b).[47] An X-ray structure of pyridine[4]arene crystals obtained from $CHCl_3$ solution in the presence of $^nBu_4NPF_6$ showed that the amide tautomer predominates, with each pyridine[4]arene binding one PF_6^- anion in an *exo* fashion by means of CH-anion and ArH-anion interactions with the alkyl groups. Two pyridine[4]arenes then come together to sandwich $CHCl_3$, which is bound in an *endo* mode. Although this type of complexation is common in the solid state, it is not typically observed in gas phase. However, DTIM-MS data for a related ternary complex measured from Me_2CO solutions of equimolar **2** and $^nBu_4NPF_6$ (Me_2CO was used for better transmission of ions to gas phase during ESI) provide definitive proof that the *exo*-complexation of the anions persists in the gas phase. DTIM is typically performed at atmospheric pressure and low electric field, enabling high resolution and accurate determination of CCS values. The CCS values for ions passing through a drift-tube filled with N_2 indicate that $[\mathbf{2}_2+PF_6+Me_2CO]^-$ and $[\mathbf{2}_2+PF_6]^-$ are clearly larger in size than are $[\mathbf{2}_2-H+Me_2CO]^-$ and $[\mathbf{2}_2-H]^-$ (Table 1). In terms of CCS values, the PF_6^- complexes are ~8 $Å^2$ larger than the deprotonated dimer (with or without included Me_2CO). The large and small effects that PF_6^- and Me_2CO respectively have on CCS are consistent with the *endo*-complexation of solvent and *exo*-complexation of anions. First observed in the solid phase, such interactions evidently persist in the gas phase.

ion	$^{DT}CCS_{N2}$ ($Å^2$)	IM d[a] (nm)	DOSY d[b] (nm)	X-ray / molecular model d (nm)
$[\mathbf{2}_2-H]^-$	389.8	2.2	2.0	1.9
$[\mathbf{2}_2-H+Me_2CO]^-$ [47]	388.6	2.2		
$[\mathbf{2}_2+PF_6]^-$	396.9	2.3		
$[\mathbf{2}_2+PF_6+Me_2CO]^-$	397.6	2.3		

$[Pd_3L^4_6]^{6+}$	1106–1192	3.8	3.6	3.9[c]

[a] Calculated from the CCS assuming a spherical conformation

[b] Based on the Stokes–Einstein equation

[c] Obtained from molecular modelling.

Table 1 | **A comparison of ionic diameters from IM, ^{1}H DOSY NMR, X-ray diffraction and molecular modelling.**[47,60,63] The collission cross-section (CCS) values were each obtained using an N_2-filled drift tube ion mobility (IM) spectrometer.

Self-interlocked structures such as catenanes and [1]rotaxanes are special examples of host–guest systems. Interlocked structures in general have been of interest in recent years for their potential as molecular switches and machines, and such research contributed partly to the 2016 Nobel Prize in Chemistry. The operation of a molecular switch relies on it being able to exist in two or more discrete structural states that do not interconvert unless an external stimulus is applied. For example, the [1]pseudorotaxane $[\mathbf{3}]^+$ features a redox-active tetrathiafulvalene unit, to which is attached a benzylammonium fragment whose threading through a pendant crown ether is under redox control (FIG. 4a).[49] The tetrathiafulvalene undergoes two $1e^-$ oxidations, such that the [1]pseudorotaxane can exist in three charge states $[\mathbf{3}]^{3+/2+/+}$, each of which is observed in ESI mass spectra. When subjected to TWIM-MS, $[\mathbf{3}]^+$ gives rise to two peaks in arrival time distributions (peaks centred at 9.45 ms and 10.25 ms), corresponding to non-threaded and threaded structures (FIG. 4b). The threaded structure is larger because the naphalene group must extend away from the tetrathiafulvalene to enable threading of the benzylammonium through the crown ether. Preceding the TWIM cell is an ion trap, and one can increase the collision energy here to increase the internal energy of $[\mathbf{3}]^+$ such that more of it is present in the unthreaded instead of the threaded state. With respect to the different charge states $[\mathbf{3}]^{3+/2+/+}$, unthreading is most favoured for the most oxidized species $[\mathbf{3}]^{3+}$ because the dicationic tetrathiafulvalene repels the benzylammonium group and participates in favourable π–π stacking interactions with the electron-rich naphthalene (FIG. 4c). The results from TWIM-MS are consistent with those from cyclic voltammetry, such that we can confirm (rather than assume) the occurrence of supramolecular phenomena in the gas phase.[42]

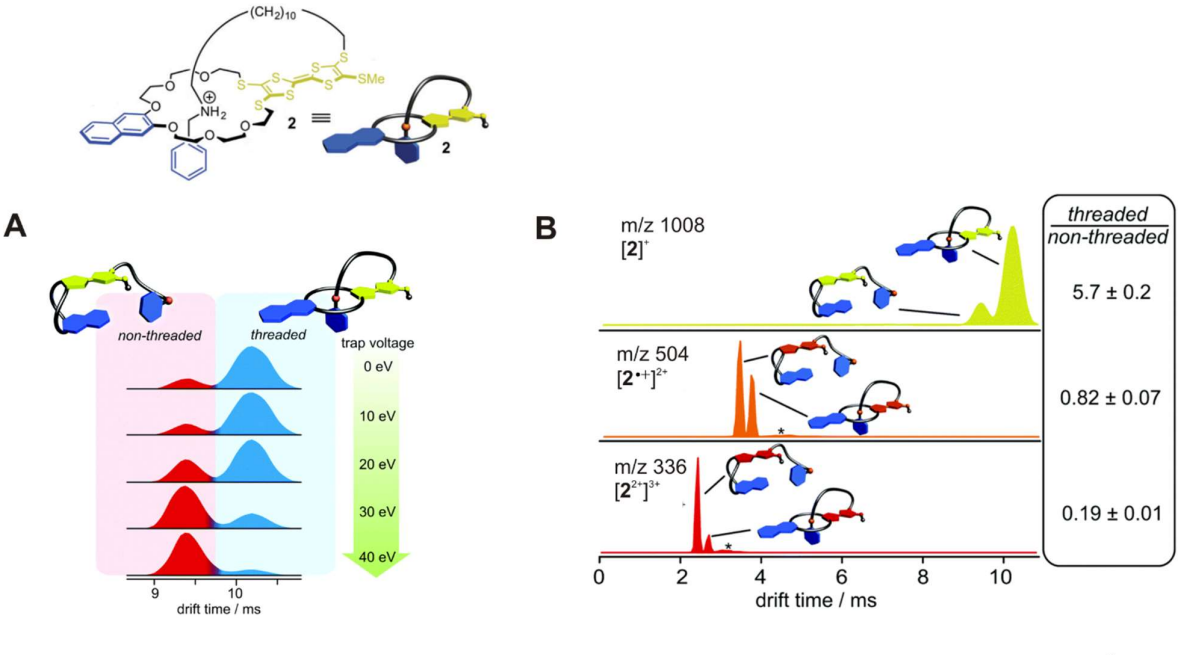

Figure 4 | **Redox-triggered threading of [1]pseudorotaxane can be observed using ion-mobility spectrometry. a** | The [1]pseudorotaxane $[\mathbf{3}]^{+}$ features an benzylammonium group inside a dithio crown ether. **b** | The normalized IM spectra of $[\mathbf{3}]^{+}$ (*m/z* 1008) after collision-induced dissociation (CID) experiments show that increasing trap voltages (collision energies) cause unthreading. **c** | The spectra for the different charge states $[\mathbf{3}]^{+}$, $[\mathbf{3}]^{2+}$ and $[\mathbf{3}]^{3+}$ suggest that oxidation is accompanied by unthreading. Figure adapted with permission from REF. 49, Royal Society of Chemistry.

[H1] Metallosupramolecular complexes

The self-assembly of organic ligands and metal centres — of which transition metal cations are the most popular — leads to metallosupramolecular structures such as dimeric or multimeric capsules, molecular polyhedra, simple coordination complexes, metallopolymers or metal–organic frameworks. In many cases, by making use of a suitably soft ionization process such as ESI, MS analysis can answer questions about molecular constitution and stoichiometry, including telling us how many of each subunit are included in a complex. Additionally, if we perform IM analysis we can obtain information on conformational dynamics and structural/conformational monodispersivity. In some cases, IM-MS can even reveal the existence of higher nuclearity complexes that are unobservable in mass spectra due to their low abundance and overlapping *m/z* values.[50,51] Indeed, TWIM-MS analysis of self-assembly products of tritopic tris(2,2′:6′,2″-terpyridine) ligand $\mathbf{L^1}$ and Zn^{2+} revealed the formation of $\{Zn_9\mathbf{L^1}_6\}$ as well as a smaller structure $\{Zn_6\mathbf{L^1}_4\}$ (REF.[52]). Although the two complexes can be identified by their different ion progressions in the MS data, IM is essential when it comes to separating the complexes with overlapping *m/z* values, such as $\{[Zn_9\mathbf{L^1}_6](PF_6)_9\}^{9+}$ and $\{[Zn_6\mathbf{L^1}_4](PF_6)_6\}^{6+}$ (*m/z* 1217.5) (FIG. 5a).

The resolution of complexes with overlapping isotopic patterns is undoubtedly valuable, but arguably the most important information that comes from IM data is that regarding the topology of a self-assembled system — whether it is a cluster,[55] capsule,[56] metallocycle[57-60] or cage.[61] Even when an X-ray structure has been determined, IM-MS data remain important because they reflect bulk properties in gas phase and can indicate the presence of various topologies or structural isomers.[53,62] This topological information is obviously even more crucial when an X-ray crystal structure of the system is not available. For example, the dimeric capsule structure of $[Ag_4\mathbf{L^2}_2]^{4+}$, where $\mathbf{L^2}$ is a tetrakis(pyridyl) ligand, could be confirmed crystallographically[56], but that of the related iodonium $[I_4\mathbf{L^2}_2]^{4+}$ could not. However, TWIM-MS analysis of the dications $\{[Ag_4\mathbf{L^2}_2](OTs)_2\}^{2+}$ and $\{[I_4\mathbf{L^2}_2](OTs)_2\}^{2+}$ afforded ATDs where peaks were centered at 8.49 ms, consistent with the I^I complex being isostructural to the Ag^I capsule dimer complex.

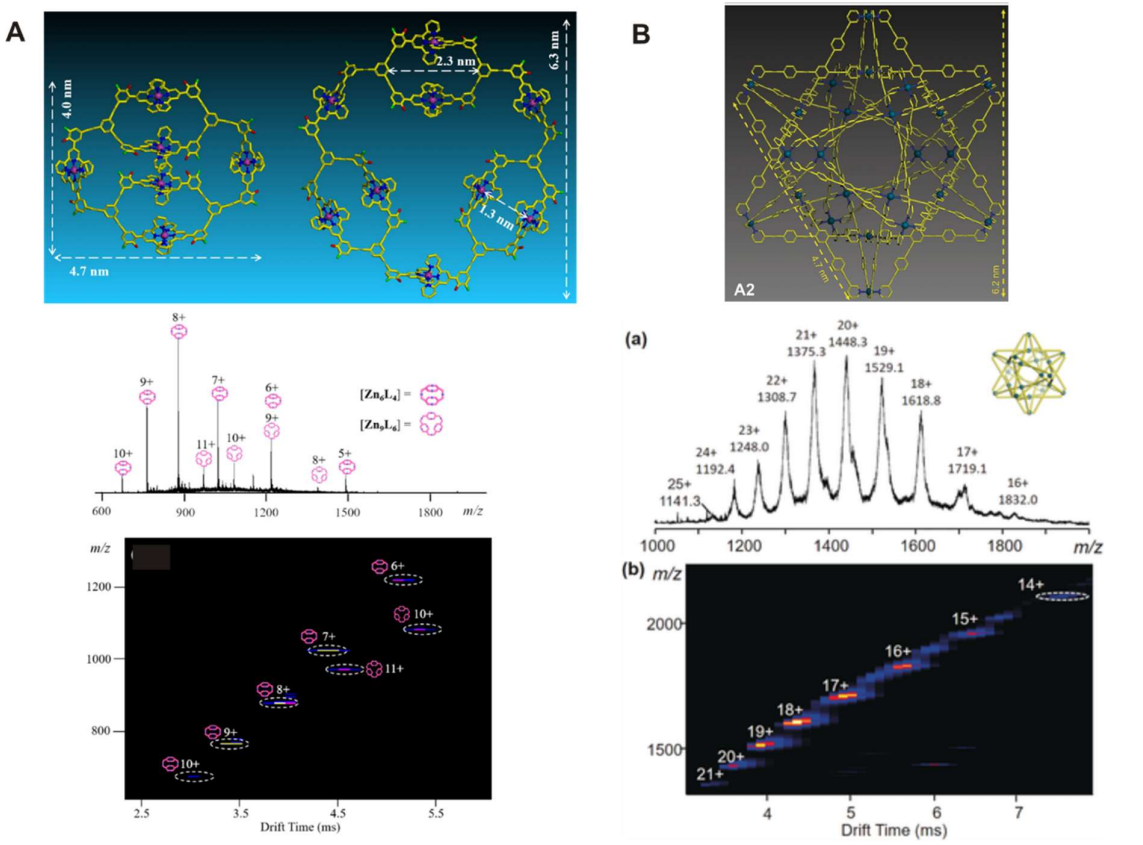

Figure 5 | **Ion-mobility mass spectrometry can help us identify complexes with overlapping m/z values and isotopic patterns. Aa** | Schematic depictions of $[Zn_6\mathbf{L^1}_4]^{12+}$ and $[Zn_9\mathbf{L^1}_6]^{18+}$, along with the dimensions of their energy-minimized structures **Ab** | ESI-MS and 2D IM-MS spectra of the complexes, annotated with the charge states of the intact assemblies. **Ba** | A schematic depiction of the 3D Star of David complex $[Pd_{24}\mathbf{L^3}_{24}]^{48+}$. ESI-MS and 2D IM-MS spectra of the complex. Part **a** reproduced with permission from REF. 52, American Chemical Society. Part **b** reproduced with permission from REF. 53, Wiley-VCH.

An aesthetically pleasing finding regards the structures of 2D (Pt^{II}) and 3D (Pd^{II}) Star of David complexes (FIG. 5b).[53] Remarkably, the 3D Star of David $[Pd_{24}\mathbf{L}^{3}_{24}]^{48+}$ forms as the only product from equimolar $\mathbf{L}^{3}$ and Pd^{II}, despite its huge experimental weight of 30,681 Da (e.g. *m/z* 1448.3 for $\{[Pd_{24}\mathbf{L}^{3}_{24}](BF_4)_{28}\}^{20+}$). Here, it is DTIM-MS analysis that showed a single series of bands for each charge state, each with a narrow drift time. In contrast, certain charge states of Ag thiolate clusters $[Ag_n(SR)_m]$ (for example, $[Ag_{44}(SR)_{30}]^{3-/4-}$) have been shown by IM-MS to exist in several different isomeric forms in the gas phase.[63]

A particularly useful application of IM-MS relates to monitoring structural changes in metal coordination cages or molecular polyhedra, including those triggered by an external stimulus. The flower-like 'superchiral' compound $[Pd_3\mathbf{L}^{4}_{6}]X_6$ (FIG. 6a; $X^- = NO_3^-$ or BF_4^-), which contains 60 chiral centres and non-coordinating anions,[64] converts into the smaller cyclic trimer $[Pd_3\mathbf{L}^{4}_{3}Cl_6]$ on complexation of Cl^- anions. The transformation can be reversed by abstracting the Cl^- ligands using a Ag^I salt. As one would expect, DTIM-MS gives CCS values that gradually decrease as one adds successive Cl^- ions to the structurally monodisperse species $[Pd_3\mathbf{L}^{4}_{6}]X_6$. This is because three of the large organic ligands are each sequentially replaced by two smaller Cl^- ligands. Although the charge-neutral complex $[Pd_3\mathbf{L}^{4}_{3}Cl_6]$ is not detectable by MS, addition of $AgBF_4$ fully transforms it back to the parent complex $[Pd_3\mathbf{L}^{4}_{6}]^{6+}$, whose size, conformational flexibility and chirality are reminiscent of small proteins. Contrary to the rigid pyridyl donors in the examples above,[52,54,65] ligand $\mathbf{L}^{4}$ affords conformationally flexible species that give rise to the many features in the IM spectrum (FIG. 6a).

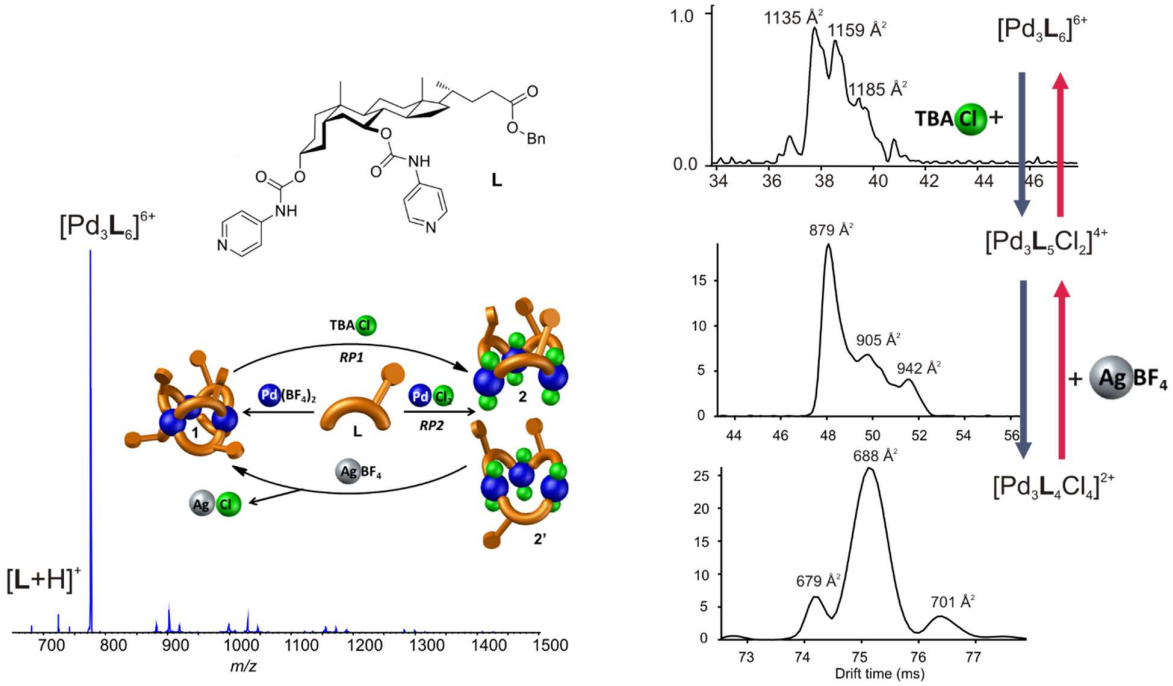

Figure 6 | **A chiral ditopic briding ligand can be displaced by Cl^- ions to afford complexes with greater ion mobilities. a** | The ESI mass spectrum of $[Pd_3\mathbf{L}^{4}_{6}](BF_4)_6$ (5 μM in CH_3CN) and schematic

of its conversion to two isomers of $[Pd_3\mathbf{L^4}_3Cl_6]$. **b** | IM spectra for $[Pd_3\mathbf{L^4}_6]^{6+}$, $[Pd_3\mathbf{L^4}_5Cl_2]^{4+}$ and $[Pd_3\mathbf{L^4}_4Cl_4]^{2+}$ formed after addition of ^{n}Bu$_4$NCl.[64] Figure reproduced with permission from REF. 64, Wiley-VCH.

[H1] Conclusions and outlook

Mass spectrometry is a useful tool for characterizing elaborate supramolecular complexes and assemblies. Although many such species are labile, they are amenable to analysis using soft ionization methods such as ESI, which can be sufficiently mild so as not to compromise the structural integrity of analytes. The sample preparation for ESI-IM-MS analysis does not differ to that for ESI-MS, such that it is very convenient to obtain the rich structural information provided by IM. There exist well-established IM-MS protocols for biomolecules, including native proteins, but the same cannot be said for supramolecular complexes and assemblies. The relatively weak forces holding these species together, from hydrophobic interactions to electrostatic forces and metal–ligand coordination, must be taken into account when optimizing experimental conditions such as solvent, concentration, temperature and ion source voltages. For example, hydrogen-bonded systems are disrupted by protic (or moderately Brønsted basic) solvents, while halogen-bonded systems can fall apart if a strong halogen bond acceptor like MeCN is used. Samples that contain H_2O may experience changes in pH during ESI, affecting the chemistry responsible for self-assembly. While many biomolecular samples are measured as their aqueous-based solutions, this is less of a problem for synthetic assemblies because they are often measured in volatile polar solvents. MS is only amenable to the analysis of charged analytes —salts or species that can readily bind/lose ions during ionization. In the latter case, we must be carefully evaluate if the reaction leading to a charged species influences the supramolecular interactions in the initial charge-neutral species. For example, if a hydrogen bond acceptor is protonated during ionization it becomes much less basic.

We must keep in mind that supramolecular systems can be dynamic in solution and often have components with only modest association constants. Thus, if the initial system concentration is low, it can dissociate (to some extent) into free individual components or lower nuclearity species. Indeed, the typical sample concentration used for ESI-MS (< 10–20 μM) may be below the association threshold for the complex. Using higher concentrations would encourage self-assembly but can have the disadvantage of leading to false positive findings due to non-specific clustering during the desolvation process. In general, we must take into account any changes in interaction strengths and their structural consequences that result from ionization and desolvation. Electrostatic interactions, for example, are much stronger in the gas phase than they are in polar solvents because the latter are strong dielectric media that screen Coulombic forces.

It is important to be prudent in relating the CCS value of a supramolecular system to a structure. Just how reliable are theoretical and experimental CCS values? Although CCS values measured using DTIM are considered quite accurate (~1% error), suitable calibration still remains an issue for TWIM and TIM instruments. This is not to say that DTIM is necessarily superior — such a cell must typically be present directly after ionization, such that deliberate CID prior to IM cannot be performed with DTIM, which can additionally suffer from signal-to-noise loss when an ion gate is used.

Calculating theoretical CCS values for biological molecules is quite routine, and values are known for several members of a certain structural class. However, for abiotic supramolecular systems — especially metal coordination cages — it is much more tedious or even impossible to determine trustworthy and accurate theoretical values. Only through the development of theoretical methods appropriate to metallosupramolecular systems will we see IM-MS methods be more informative to those studying such systems. One straightforward way to judge the reliability of and evaluate IM data is to directly compare them to structural data from methods such as DOSY NMR or single crystal X-ray diffraction. Thus, one can relate a CCS-derived diameter calculated assuming a spherical conformation of the analyte to a diameter obtained from solution DOSY NMR (computed from the hydrodynamic radius) and to the dimensions of a crystal structure (Table 1). If N_2 is used as a drift gas, the CCS-derived values agree well with the solution[57] and solid state data[50]. Although awaiting further confirmation, the relatively good agreement between the different methods underlines the utility of IM (especially DTIM, at present) to give reliable molecular diameter values even in the absence of other structural data.

Despite the rapid development of commercial IM-MS instruments, such measurements have yet to become routine in the domain of synthetic chemistry. It seems likely that the coming years will see even more developments, both in instrumentation and methodology. For the purposes of structural chemistry, improvements in DTIM-MS are particularly interesting because the method can provide CCS values without the need for cumbersome calibration procedures. It would be very advantageous for us to have access to instruments with greater IM resolving power in order to better separate subtly different conformations. Moreover, as we noted above, DTIM-MS instruments that allow pre-IM fragmentation could afford us additional structural insights. IM-MS is a technique that completes the structural chemistry palette for complex supramolecular systems, which we now can interrogate in solid, solution and gas phase. For this reason, we expect that IM-MS will have a bright future in this and other areas of chemistry research.

[H1] References

1. Avram, L. & Cohen, Y. Diffusion NMR of molecular cages and capsules. *Chem. Soc. Rev.* **44**, 586–602 (2015).

2. Rissanen, K. Crystallography of encapsulated molecules. *Chem. Soc. Rev.* **46**, 2638–2648 (2017).
3. Avram, L. & Cohen, Y. Self-assembly of resorcin[4]arene in the presence of small alkylammonium guests in solution. *Org. Lett.* **10**, 1505–1508 (2008).
4. Evan-Salem, T. & Cohen, Y. Octahydroxypyridine[4]arene self-assembles spontaneously to form hexameric capsules and dimeric aggregates. *Chem. Eur. J.* **13**, 7659–7663 (2007).
5. Cohen, Y., Evan-Salem, T. & Avram, L. Hydrogen-bonded hexameric capsules of resorcin[4]arene, pyrogallol[4]arene and octahydroxypyridine[4]arene are abundant structures in organic solvents: a view from diffusion NMR. *Supramol. Chem.* **20**, 71–79 (2008).
6. Thordarson, P. Determining association constants from titration experiments in supramolecular chemistry. *Chem. Soc. Rev.* **40**, 1305–1323 (2011).
7. von Krbek, L. K. S., Schalley, C. A. & Thordarson, P. Assessing cooperativity in supramolecular systems. *Chem. Soc. Rev.* **46**, 2622–2637 (2017).
8. Mali, K. S., Pearce, N., De Feyter, S. & Champness, N. R. Frontiers of supramolecular chemistry at solid surfaces. *Chem. Soc. Rev.* **46**, 2520–2542 (2017).
9. Hill, H. J., Eiceman, G. A. & Karpas, Z. *Ion Mobility Spectrometry*, 3rd Ed. (CRC Press, 2013). doi:10.1201/b16109
10. May, J. C., Morris, C. B. & McLean, J. A. Ion mobility collision cross section compendium. *Anal. Chem.* **89**, 1032–1044 (2017).
11. Kanu, A. B., Dwivedi, P., Tam, M., Matz, L. & Hill, H. H. Ion mobility–mass spectrometry. *J. Mass Spectrom.* **43**, 1–22 (2008).
12. Lanucara, F., Holman, S. W., Gray, C. J. & Eyers, C. E. The power of ion mobility-mass spectrometry for structural characterization and the study of conformational dynamics. *Nat. Chem.* **6**, 281–294 (2014).
13. Konijnenberg, A., Butterer, A. & Sobott, F. Native ion mobility-mass spectrometry and related methods in structural biology. *Biochim. Biophys. Acta, Proteins Proteomics* **1834**, 1239–1256 (2013).
14. Uetrecht, C., Rose, R. J., van Duijn, E., Lorenzen, K. & Heck, A. J. R. Ion mobility mass spectrometry of proteins and proteinassemblies. *Chem. Soc. Rev.* **39**, 1633–1655 (2010).
15. Bowers, M. T. Re-print of "ion mobility spectrometry: a personal view of its development at UCSB". *Int. J. Mass Spectrom.* **377**, 625–645 (2015).
16. May, J. C. *et al.* Conformational ordering of biomolecules in the gas phase: nitrogen collision cross sections measured on a prototype high resolution drift tube ion mobility-mass spectrometer. *Anal. Chem.* **86**, 2107–2116 (2014).
17. Michelmann, K., Silveira, J. A., Ridgeway, M. E. & Park, M. A. Fundamentals of trapped ion mobility spectrometry. *J. Am. Soc. Mass Spectrom.* **26**, 14–24 (2014).
18. Kaplan, K. *et al.* Resistive glass IM-TOFMS. *Anal. Chem.* **82**, 9336–9343 (2010).

19. Giles, K., Williams, J. P. & Campuzano, I. Enhancements in travelling wave ion mobility resolution. *Rapid Commun. Mass Spectrom.* **25**, 1559–1566 (2011).
20. [Duplicate of REF. 12]
21. May, J. C. & McLean, J. A. Ion mobility-mass spectrometry: time-dispersive instrumentation. *Anal. Chem.* **87**, 1422–1436 (2015).
22. Wyttenbach, T., Bleiholder, C. & Bowers, M. T. Factors contributing to the collision cross section of polyatomic ions in the kilodalton to gigadalton range: application to ion mobility measurements. *Anal. Chem.* **85**, 2191–2199 (2013).
23. Wyttenbach, T., Bleiholder, C., Anderson, S. E. & Bowers, M. T. A new algorithm to characterise the degree of concaveness of a molecular surface relevant in ion mobility spectrometry. *Mol. Phys.* **113**, 2344–2349 (2015).
24. Larriba, C. & Hogan, C. J. Free molecular collision cross section calculation methods for nanoparticles and complex ions with energy accommodation. *J. Comput. Phys.* **251**, 344–336 (2013).
25. Shvartsburg, A. A. & Jarrold, M. F. An exact hard-spheres scattering model for the mobilities of polyatomic ions. *Chem. Phys. Lett.* **261**, 86–91 (1996).
26. Siems, W. F., Viehland, L. A. & Hill, H. H. Correcting the fundamental ion mobility equation for field effects. *Analyst* **141**, 6396–6407 (2016).
27. Giles, K. *et al.* Applications of a travelling wave-based radio-frequency-only stacked ring ion guide. *Rapid Commun. Mass Spectrom.* **18**, 2401–2414 (2004).
28. Hines, K. M., May, J. C., McLean, J. A. & Xu, L. Evaluation of collision cross section calibrants for structural analysis of lipids by traveling wave ion mobility-mass spectrometry. *Anal. Chem.* **88**, 7329–7336 (2016).
29. Silveira, J. A., Michelmann, K., Ridgeway, M. E. & Park, M. A. Fundamentals of trapped ion mobility spectrometry part II: fluid dynamics. *J. Am. Soc. Mass Spectrom.* **27**, 585–595 (2016).
30. Benigni, P. *et al.* Analysis of geologically relevant metal porphyrins using trapped ion mobility spectrometry–mass spectrometry and theoretical calculations. *Energy Fuels* **30**, 10341–10347 (2016).
31. Groessl, M., Graf, S. & Knochenmuss, R. High resolution ion mobility-mass spectrometry for separation and identification of isomeric lipids. *Analyst* **140**, 6904–6911 (2015).
32. Van Berkel, G. J., Pasilis, S. P. & Ovchinnikova, O. Established and emerging atmospheric pressure surface sampling/ionization techniques for mass spectrometry. *J. Mass Spectrom.* **43**, 1161–1180 (2008).
33. Wyttenbach, T., Pierson, N. A., Clemmer, D. E. & Bowers, M. T. Ion mobility analysis of molecular dynamics. *Annu. Rev. Phys. Chem.* **65**, 175–196 (2014).
34. Allison, T. M. *et al.* Quantifying the stabilizing effects of protein–ligand interactions in the gas phase. *Nat. Commun.* **6**, 8551 (2015).

35. Stojko, J. *et al.* Ion mobility coupled to native mass spectrometry as a relevant tool to investigate extremely small ligand-induced conformational changes. *Analyst* **140**, 7234–7245 (2015).
36. Jurneczko, E. & Barran, P. E. How useful is ion mobility mass spectrometry for structural biology? The relationship between protein crystal structures and their collision cross sections in the gas phase. *Analyst* **136**, 20–28 (2011).
37. Lee, J. W., Davidson, K. L., Bush, M. F. & Kim, H. I. Collision cross sections and ion structures: development of a general calculation method *via* high-quality ion mobility measurements and theoretical modeling. *Analyst* **142**, 4289–4298 (2017).
38. *Chemistry of Nanocontainers*. (Eds. Albrecht, M & Hahn, F. E.) 1–170 (Springer Berlin Heidelberg, 2012).
39. Pinalli, R. & Dalcanale, E. Supramolecular sensing with phosphonate cavitands. *Acc. Chem. Res.* **46**, 399–411 (2013).
40. Beer, P. & Gale, P. Anion recognition and sensing: the state of the art and future perspectives. *Angew. Chem. Int. Ed.* **40**, 486–516 (2001).
41. Brotherhood, P. R. & Davis, A. P. Steroid-based anion receptors and transporters. *Chem. Soc. Rev.* **39**, 3633–3647 (2010).
42. Lee, S. J. C. *et al.* Host-guest chemistry from solution to the gas phase: an essential role of direct interaction with water for high-affinity binding of cucurbit[*n*]urils. *J. Phys. Chem. B* **117**, 8855–8864 (2013).
43. Wu, G., Olesińska, M., Wu, Y., Matak-Vinkovic, D. & Scherman, O. A. Mining 2:2 complexes from 1:1 stoichiometry: formation of cucurbit[8]uril–diarylviologen quaternary complexes favored by electron-donating substituents. *J. Am. Chem. Soc.* **139**, 3202–3208 (2017).
44. Kovalenko, E. *et al.* Supramolecular adducts of cucurbit[7]uril and amino acids in the gas phase. *J. Am. Soc. Mass Spectrom.* **27**, 265–276 (2016).
45. Lee, J. W., Shin, M. H., Mobley, W., Urbach, A. R. & Kim, H. I. Supramolecular enhancement of protein analysis via the recognition of phenylalanine with cucurbit[7]uril. *J. Am. Chem. Soc.* **137**, 15322–15329 (2015).
46. Lee, T.-C. *et al.* Chemistry inside molecular containers in the gas phase. *Nat. Chem.* **5**, 376–382 (2013).
47. Kiesilä, A. *et al.* Simultaneous *endo* and *exo* complex formation of pyridine[4]arene dimers with neutral and anionic guests. *Angew. Chem. Int. Ed.* **56**, 10942–10946 (2017).
48. [deleted]
49. Schröder, H. V., Wollschläger, J. M. & Schalley, C. A. Redox-controlled self-inclusion of a lasso-type pseudo[1]rotaxane. *Chem. Commun.* **53**, 9218–9221 (2017).
50. Brocker, E. R., Anderson, S. E., Northrop, B. H., Stang, P. J. & Bowers, M. T. Structures of metallosupramolecular coordination assemblies can be obtained by ion mobility spectrometry–mass spectrometry. *J. Am. Chem. Soc.* **132**, 13486–13494 (2010).

51. Guo, K. *et al.* Characterization of metallosupramolecular polymers by top-down multidimensional mass spectrometry methods. *Macromol. Rapid Commun.* **36**, 1539–1552 (2015).
52. Wang, L. *et al.* Self-assembly of tetrameric and hexameric terpyridine-based macrocycles using Cd(II), Zn(II), and Fe(II). *Inorg. Chem.* **57** (7) 3548–3558 (2018).
53. Song, B. *et al.* Direct self-assembly of a 2D and 3D Star of David. *Angew. Chem. Int. Ed.* **56**, 5258–5262 (2017).
54. Ujma, J. *et al.* Shapes of supramolecular cages by ion mobility mass spectrometry. *Chem. Commun.* **48**, 4423–4425 (2012).
55. Myung, S., Julian, R. R., Nanita, S. C., Cooks, R. G. & Clemmer, D. E. Formation of nanometer-scale serine clusters by sonic spray. *J. Phys. Chem. B* **108**, 6105–6111 (2004).
56. Turunen, L. *et al.* [N···I$^+$···N] Halogen-bonded dimeric capsules from tetrakis(3-pyridyl)ethylene cavitands. *Angew. Chem. Int. Ed.* **55**, 14033–14036 (2016).
57. Chan, Y.-T. *et al.* Self-assembly and traveling wave ion mobility mass spectrometry analysis of hexacadmium macrocycles. *J. Am. Chem. Soc.* **131**, 16395–16397 (2009).
58. Perera, S. *et al.* Hexameric palladium(II) terpyridyl metallomacrocycles: assembly with 4,4′-bipyridine and characterization by TWIM mass spectrometry. *Angew. Chem. Int. Ed.* **49**, 6539–6544 (2010).
59. Chan, Y.-T. *et al.* Design, synthesis, and traveling wave ion mobility mass spectrometry characterization of iron(II)– and ruthenium(II)–terpyridine metallomacrocycles. *J. Am. Chem. Soc.* **133**, 11967–11976 (2011).
60. Li, Y. *et al.* Giant, hollow 2D metalloarchitecture: stepwise self-assembly of a hexagonal supramolecular nut. *J. Am. Chem. Soc.* **138**, 10041–10046 (2016).
61. Bonakdarzadeh, P. *et al.* DOSY NMR, X-ray structural and ion-mobility mass spectrometric studies on electron-deficient and electron-rich M_6L_4 coordination cages. *Inorg. Chem.* **54**, 6055–6061 (2015).
62. Baker, E. S. *et al.* Probing shapes of bichromophoric metal–organic complexes using ion mobility mass spectrometry. *J. Am. Chem. Soc.* **127**, 18222–18228 (2005).
63. Baksi, A. *et al.* Isomerism in monolayer protected silver cluster ions: an ion mobility-mass spectrometry approach. *J. Phys. Chem. C* **121**, 13421–13427 (2017).
64. Jurček, O. *et al.* Superchiral Pd_3L_6 coordination complex and its reversible structural conversion into $Pd_3L_3Cl_6$ metallocycles. *Angew. Chem. Int. Ed.* **54**, 15462–15467 (2015).
65. Wang, C. *et al.* Self-assembly of giant supramolecular cubes with terpyridine ligands as vertices and metals on edges. *Chem. Sci.* **5**, 1221–1226 (2014).
66. Carroy, G. *et al.* Influence of equilibration time in solution on the inclusion/exclusion topology ratio of host–guest complexes probed by ion mobility and collision-induced dissociation. *Chem. Eur. J.* **22**, 4528–4534 (2016).